Strain Hardening in Polymer Glasses: Limitations of Network Models

Robert S. Hoy* and Mark O. Robbins

Department of Physics and Astronomy, Johns Hopkins University, Baltimore, MD 21218
(Dated: May 29, 2007)

Simulations are used to examine the microscopic origins of strain hardening in polymer glasses. While traditional entropic network models can be fit to the total stress, their underlying assumptions are inconsistent with simulation results. There is a substantial energetic contribution to the stress that rises rapidly as segments between entanglements are pulled taut. The thermal component of stress is less sensitive to entanglements, mostly irreversible, and directly related to the rate of local plastic arrangements. Entangled and unentangled chains show the same strain hardening when plotted against the microscopic chain orientation rather than the macroscopic strain.

The stress needed to deform a polymer glass increases as the strain rises. This strain hardening plays a critical role in stabilizing polymers against strain localization and fracture, and reduces wear [1]. While models have had some success in fitting experimental data, fundamental inconsistencies in fit parameters and trends imply that our understanding of the microscopic origins of strain hardening is far from complete.

Most theories of strain hardening [2, 3] are based on rubber elasticity theory [4]. These entropic network models assume that polymer glasses behave like crosslinked rubber, with the number of monomers between crosslinks equal to the entanglement length N_e. The increase in the stress σ due to deformation by a stretch tensor $\bar{\lambda}$ is attributed to the decrease in entropy as polymers are stretched between affinely displaced entanglements. One finds [3]

$$\sigma(\bar{\lambda}) = \sigma_0 + G_R g(\bar{\lambda}) L^{-1}(h)/3h \qquad (1)$$

where σ_0 is the yield or plastic flow stress, G_R is the strain hardening modulus, L^{-1} is the inverse Langevin function, $g(\bar{\lambda})$ describes the entropy reduction for Gaussian chains, and $L^{-1}(h)/3h$ corrects for the finite length of segments between entanglements. The value of N_e enters in h, which is the ratio of the Euclidean distance between entanglements to the contour length.

Stress-stretch curves for a wide variety of glassy polymers can be fit to Eq. 1, but the fit parameters are not consistent with the microscopic picture underlying entropic network models [5]. For example, values of N_e from fitting h may be several times smaller than those obtained from the plateau modulus G_N^0 [3]. Entropic network models predict $G_R \approx G_N^0$ near T_g, but measured G_R are about 100 times larger [6]. G_R also rises as T decreases [6, 7], while any entropic stress must drop to zero as $T \to 0$ [5]. Recent work [7, 8] shows that changes in G_R correlate with those in the plastic flow stress. Indeed entire stress-stretch curves collapse when normalized by σ_0 [7]. This is not expected from entropic models, where σ_0 is treated as an independent parameter arising from local plasticity. A more conceptual difficulty in entropic models is that, unlike rubber, glasses are not able to dynamically sample chain conformations.

In this Letter we use simulations to examine the microscopic origins of strain hardening. While our results for the total stress can be fit to Eq. 1, network models are not consistent with observed changes in energy, heat flow and molecular conformations. The stress can be divided into energetic and thermal contributions. The energetic contribution is strictly zero in the entropic model, but we find it becomes significant as the segments between entanglements are stretched taut. In contrast, entanglements have little direct influence on the thermal contribution. This thermal stress is found to be directly related to the rate of local plastic rearrangements. Finally, network models only predict strain hardening for entangled chains ($N \gg N_e$), yet substantial hardening is observed for N as small as $N_e/4$. Results for entangled and unentangled chains collapse when plotted as a function of the microscopic strain-induced orientation of chains rather than the macroscopic strain.

Much of the physics of polymer glasses is independent of chemical detail [3, 9, 10]. We thus employ a simple coarse-grained bead-spring model [11] that captures the key physics of linear homopolymers. Each polymer chain contains N beads of mass m. All beads interact via the truncated and shifted Lennard-Jones potential $U_{LJ}(r) = 4u_0[(a/r)^{12} - (a/r)^6 - (a/r_c)^{12} + (a/r_c)^6]$, where $r_c = 1.5a$ is the cutoff radius and $U_{LJ}(r) = 0$ for $r > r_c$. We express all quantities in terms of the molecular diameter a, binding energy u_0, and characteristic time $\tau_{LJ} = \sqrt{ma^2/u_0}$.

Covalent bonds between adjacent monomers on a chain are modeled using the finitely extensible nonlinear elastic potential $U(r) = -(1/2)(kR_0^2)ln(1 - (r/R_0)^2)$, with the canonical parameter choices $R_0 = 1.5a$ and $k = 30u_0/a^2$ [11]. Chain stiffness is introduced through a bending potential $U_{bend}(\theta) = k_{bend}(1 - cos\theta)$, where θ is the angle between consecutive covalent bond vectors along a chain. Stiffer chains have lower entanglement lengths. Values of N_e obtained from primitive path analysis (PPA) [12] range from $N_e = 71$ for flexible chains ($k_{bend} = 0$) to $N_e = 22$ for $k_{bend} = 2.0u_0$.

Glassy states were obtained by rapid temperature quenches from well-equilibrated melts [13] to a temperature T below the glass transition temperature $T_g \simeq$

$0.35u_0/k_B$ [14]. While quench rate affects the initial yield stress [15], it had little influence on strain hardening. Periodic boundary conditions were imposed, with periods L_i along directions $i = x$, y, and z. The initial periods L_i^0 were chosen to give zero pressure at T. A Langevin thermostat with damping rate $1/\tau_{LJ}$ was applied to the peculiar velocities in all three directions.

Experiments commonly impose compressive deformations because they suppress strain localization [6, 10, 16]. Simulations were performed for both uniaxial and plane strain compression. Both show the same behavior, and only uniaxial results are presented below. The cell is compressed along z at constant true strain rate $\dot{\epsilon} = \dot{L_z}/L_z$. Results for $\dot{\epsilon} = -10^{-5}/\tau$ are shown below, but similar behavior is found at $\dot{\epsilon} = -10^{-3}/\tau$. Qualitative changes can occur at the higher rates employed in recent atomistic simulations of strain hardening [17, 18, 19, 20]. The stress perpendicular to the compressive axis is maintained at zero by varying L_x and L_y [21]. Fits to network models normally assume that the volume remains constant and $L_x = L_y$ and this is approximately true in our simulations. Then deformation can be expressed in terms of a single stretch component $\lambda \equiv L_z/L_z^0$.
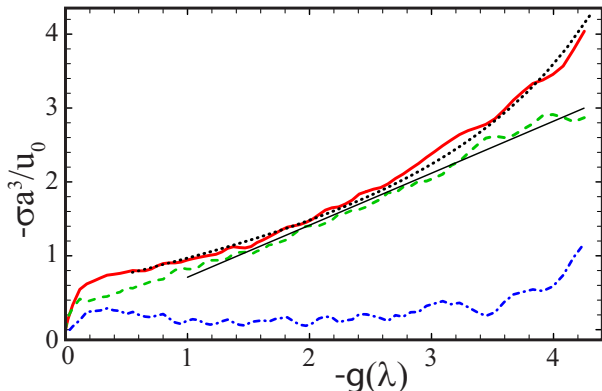

FIG. 1: (Color online) Total stress (solid line) and contributions from heat (dashed line) and potential energy (dot-dashed line) for a system with $T = 0.2u_0/k_B$, $N = 350$ and $N_e = 22$. Fits of σ to Eq. 1 with $N_e = 13$ (dotted line) and of σ_Q to a straight line are also shown. Both σ and g are negative under compression.

Typical strain hardening results are shown in Fig. 1. As in experiments, the stress is plotted against $g(\lambda) \equiv \lambda^2 - 1/\lambda$. Then entropic network models (Eq. 1) attribute curvature in the strain hardening regime to reductions in entropy associated with the finite length N_e between entanglements. The strong upward curvature in Fig. 1 can be fit to Eq. 1 (dotted line), but with a value of $N_e = 13$ that is much smaller than that determined from G_N^0 or PPA ($N_e = 22$). Similar reductions are found for other chain stiffnesses and in fits to experiment.

The stress represents the incremental work done on a unit volume of the system by an incremental strain. It can be divided into contributions from changes in the internal energy density U and the heat flow out of a unit volume Q: $\sigma = \sigma_U + \sigma_Q$ where $\sigma_U = \partial U/\partial\epsilon$ and $\sigma_Q = \partial Q/\partial\epsilon$. The derivation of Eq. 1 assumes that σ_U does not contribute to strain hardening and that σ_Q is entirely due to reversible heat associated with changes in entropy. Simulations allow these assumptions to be tested.

Figure 1 shows that results for σ_Q can be fit to the linear behavior predicted for the entropy of ideal Gaussian chains at $|g| > 1$. Fits to smaller $|g|$ can be obtained with $N_e = 30$ in Eq. 1, but fits to uniaxial and plane strain results always give N_e that are larger than values obtained from G_N^0 and PPA, and much larger than values from fits to the total stress. Separate simulations show that σ_Q is dominated by irreversible heat flow rather than changes in entropy. After straining to a large $|g|$ the stress is returned to zero. The stretch only relaxes about 10% and only $\sim 5\%$ of the work associated with σ_Q is recovered. Similar irreversibility is observed in experiments [16], confirming that the force can not be entropic.

The energetic contribution to the stress in Fig. 1 is important during the initial rise to the plastic flow stress σ_0. The value of σ_U then drops to a small constant for $0.5 < |g| < 2.5$. At larger strains there is a pronounced upturn in σ_U that contributes almost all of the curvature in the total stress. This energetic term thus has a crucial effect on fit values of N_e even though the derivation of Eq. 1 assumes $\sigma_U = 0$. Similar results are found for all T and k_{bend}, and for uniaxial and plane strain. In all cases, σ_Q exhibits nearly ideal Gaussian behavior ($L^{-1}(h)/3h \simeq 1$) and σ_U leads to a more rapid rise in stress at large stretches. The effect of σ_U increases and extends to smaller $|g|$ as the intrinsic N_e from PPA decreases.

Examination of the evolving conformations of individual chains also provides tests of entropic network models. If entanglements act like crosslinks, then polymer glasses should deform affinely on scales greater than the entanglement spacing. Our recent studies confirm this affine displacement, and the associated increase in h as segments between entanglements pull taut [7]. Fig. 1 shows that this increase in h has little effect on the thermal terms that motivated Eq. 1. Instead, straightening of segments produces large energetic terms by disrupting the local packing structure. Energy is stored in increasing tension in the covalent bonds countered by compression of intermolecular bonds. Experiments also find significant energy storage [16, 22], and could in principal track σ_U over the full strain hardening regime.

Further insight into strain hardening is provided by examining the dependence on chain length. Entropic network models assume that the length should not matter for highly entangled systems, $N \gg N_e$, and there should be no network to produce strain hardening for $N < N_e$. Simulations confirm that σ is independent of N for $N \gg N_e$, but show substantial strain hardening

for $N < N_e$ [7, 17]. Figure 2(a) illustrates this hardening for chains as short as $N_e/4$. Results for short chains follow the asymptotic behavior of highly entangled chains ($N/N_e > 4$) to larger $|g|$ as N increases. This suggests that deformation changes chain conformations on longer scales as $|g|$ increases and that entanglements only become relevant at large $|g|$ ($|g| \gtrsim 2.5$ in Fig. 2).

The observation of strain hardening implies that the microscopic arrangement of chains evolves under stretching. One way of quantifying this is through changes in the root mean squared components R_i of the end-to-end vectors of chains relative to their initial values R_i^0. Under an affine deformation at constant volume: $\lambda = R_z/R_z^0 = (R_x^0/R_x)^2 = (R_y^0/R_y)^2$. The deformation of short chains is subaffine[7, 23], but we find that the above ratios [24] can all be described by an effective stretch λ_{eff} [25]. Figure 2(b) shows $g(\lambda_{eff})$ as a function of $g(\lambda)$ for different N. All chains show significant stretching, and highly entangled systems deform affinely. The small deviation between g(λ) and g(λ_{eff}) for $N \gg N_e$ results from a small increase in density ($\sim 4\%$) at large $|g|$ rather than nonaffine deformation. As N decreases, the deformation becomes subaffine at smaller and smaller $|g|$. This confirms that the scale over which chain conformations are distorted grows with $|g|$, and that entanglements only become important for $|g| \gtrsim 2.5$ in this system.

Strain hardening is directly related to the changes in chain conformation represented by λ_{eff} rather than the macroscopic deformation λ [25]. To illustrate this, data from Fig. 2(b) are replotted against $g(\lambda_{eff})$ in Fig. 2(c). Data for different chain lengths collapse onto a single curve even though N is as much as 4 times smaller than N_e. Similar results are found for other T, N_e and for plane strain compression. Deviations are only seen when N becomes comparable to the persistence length and chains can no longer be viewed as Gaussian random walks. These results show that entanglements do not have a direct effect on strain hardening. Their main role appears to be in forcing the local stretching of chains λ_{eff} to follow the global stretch λ.

The recently observed [7, 8] correlation between the strain hardening modulus G_R and the plastic flow stress σ_0 suggests that local plastic rearrangements dissipate most of the energy during compression. To monitor the rate of plasticity $P \equiv \delta f/\delta\epsilon$, we counted the fraction δf of Lennard-Jones bonds with $r < r_c$ whose length changed by more than 20% over small intervals in strain $\delta\epsilon = 0.005$. Tests on this and related amorphous models [26] show that this criterion is large enough to exclude elastic deformations, and that $\delta\epsilon$ is small enough that a given bond does not undergo multiple events. To eliminate plastic rearrangements associated with equilibrium aging, the rate of plasticity during deformation was monitored at $T = 0$.

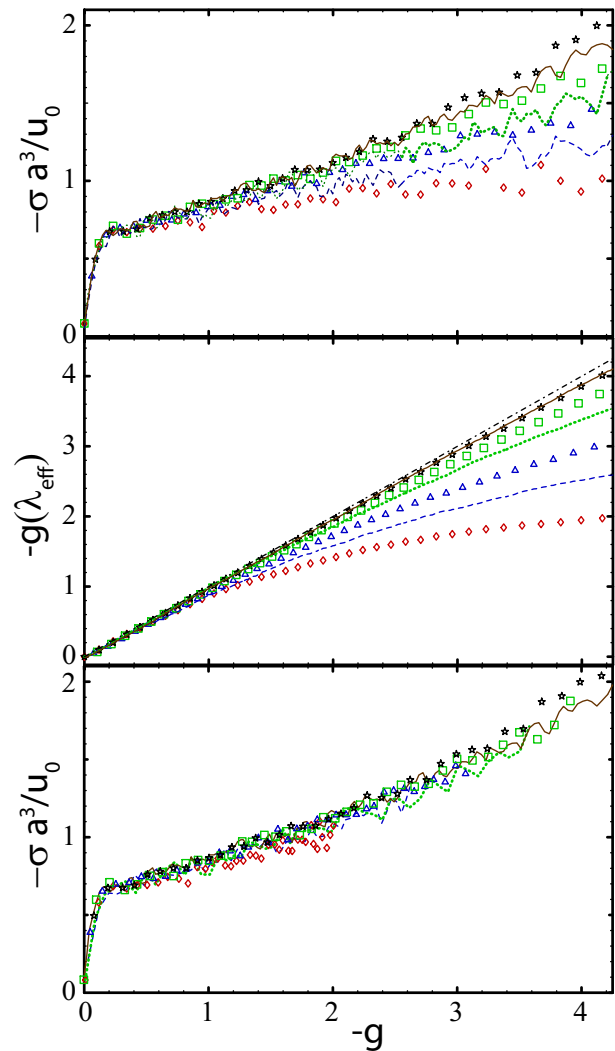Figure 3 shows the rate of plasticity for $N_e = 26$ and

FIG. 2: (Color online) (a) Stress vs. $g(\lambda)$ during uniaxial compression at $k_B T = .2u_0$ for $k_{bend} = 0.75u_0$, $N_e = 39$ and strain rate $\dot{\epsilon} = -10^{-5}/\tau_{LJ}$. Successive curves from bottom to top are for N = 10 ($\diamond$), 16 ($- - -$), 25 ($\triangle$), 40 ($\cdots$), 70 (squares), 175 ($-$), and 350 ($\star$). (b) $g(\lambda_{eff})$ vs. $g(\lambda)$ for the same systems. The dot-dashed line corresponds to $\lambda_{eff} = \lambda$. (c) Stresses for different N collapse when plotted against $g(\lambda_{eff})$.

71. There is a rapid initial rise as σ approaches σ_0, followed by a nearly linear increase during the strain hardening regime. Also plotted in Fig. 3 are results for σ_Q. A fixed vertical rescaling (coincidentally close to unity in our units) produces an excellent collapse of P and σ_Q for all N_e. Note that even the fluctuations in the quantities are correlated [27]. Similar results are found for other criteria for the rate of plasticity, with only the scaling factor changing.

The above results clearly illustrate that the thermal contribution to strain hardening is associated with an increase in the rate of plastic rearrangements as chains stretch. It remains unclear why this increase should ap-
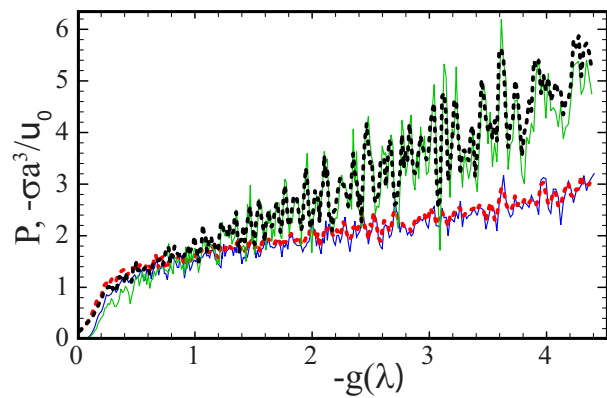
FIG. 3: (Color online) Rate of plastic rearrangements P (solid lines) as a function of $g(\lambda)$ for $N_e = 26$ (upper curve) and 71 (lower curve) at $k_B T = 0u_0$. Dashed lines show the corresponding dissipative stress σ_Q.

proximately follow the increase in entropic stress predicted for Gaussian chains. The entropic stress represents the rate of decrease in the logarithm of the number of available chain conformations. One possibility is that the rate of plastic rearrangements scales in the same way because a decrease in the number of conformations necessitates larger scale plastic rearrangements. The relationship between the plastic flow stress and hardening modulus follows naturally from this picture, and it also explains why data for different chain lengths collapse when plotted against λ_{eff}. Analytic investigations of this scenario may prove fruitful.

Our results for σ_U suggest that the success of Eq. 1 in fitting the total stress may be coincidental, and explain why fit values of N_e are generally smaller than intrinsic values from G_N^0 and PPA. It would be interesting to compare trends in the calculated σ_U and σ_Q to experimental results. These could be obtained by differentiating deformation calorimetry results for the work and heat, but existing studie s have only extended to the plastic flow regime [28, 29, 30].

---

* Electronic address: robhoy@pha.jhu.edu

[1] Y. J. Mergler and R. P. Schaake, J. Appl. Polym. Sci. **92**, 2689 (2004).

[2] R. N. Haward and G. Thackray, Proc. Roy. Soc. Lond. **302**, 453 (1968).

[3] E. M. Arruda and M. C. Boyce, Int. J. Plast. **9**, 697 (1993).

[4] L. R. G. Treloar, *The Physics of Rubber Elasticity* (Clarendon Press, Oxford, 1975).

[5] E. J. Kramer, J. Polym. Sci. Part B: Polym. Phys. **43**, 3369 (2005).

[6] H. G. H. van Melick, L. E. Govaert, and H. E. H. Meijer, Polymer **44**, 2493 (2003).

[7] R. S. Hoy and M. O. Robbins, J. Polym. Sci. Part B - Polymer Phys. **44**, 3487 (2006).

[8] R. B. Dupaix and M. C. Boyce, Polymer **46**, 4827 (2005).

[9] R. N. Haward and R. J. Young, eds., *The Physics of Glassy Polymers, 2nd edition* (Chapman and Hall, London, 1997).

[10] R. N. Haward, Macromolecules **26**, 5860 (1993).

[11] K. Kremer and G. S. Grest, J. Chem. Phys. **92**, 5057 (1990).

[12] R. Everaers, S. K. Sukumaran, G. S. Grest, C. Svaneborg, A. Sivasubramanian, and K. Kremer, Science **303**, 823 (2004).

[13] R. Auhl, R. Everarers, G. S. Grest, K. Kremer, and S. J. Plimpton, J. Chem. Phys. **119**, 12718 (2003).

[14] J. Rottler and M. O. Robbins, Phys. Rev. E **68**, 011507 (2003).

[15] J. Rottler and M. O. Robbins, Phys. Rev. Lett. **95**, 225504 (2005).

[16] O. A. Hasan and M. C. Boyce, Polymer **34**, 5085 (1993).

[17] A. V. Lyulin, N. K. Balabaev, M. A. Mazo, and M. A. J. Michels, Macromolecules **37**, 8785 (2004).

[18] At sufficiently high rates, chains are constrained to deform affinely. This gives $\lambda_{eff} = \lambda$ and the shear stress is nearly independent of $\dot{\epsilon}$. Thus the conclusion that strain hardening is controlled by λ_{eff} also applies in this limit.

[19] A. V. Lyulin, B. Vorselaars, M. A. Mazo, N. K. Balabaev, and M. A. J. Michels, Europhys. Lett, **71**, 618 (2005).

[20] J. Li, T. Mulder, B. Vorselaars, A. V. Lyulin, and M. A. J. Michels, Macromolecules **39**, 7774 (2006).

[21] L. Yang, D. J. Srolovitz, and A. F. Yee, J, Chem. Phys **107**, 4396 (1997).

[22] C. Chui and M. C. Boyce, Macromolecules **32**, 3795 (1999).

[23] M. Dettenmaier, A. Maconnachie, J. S. Higgins, H. H. Kaush, and T. Q. Nguyen, Macromolecules **19**, 773 (1986).

[24] All three ratios give the same value of λ_{eff} when the chains are long compared to their persistence length. For shorter chains the best correlation is found by using results for the stretched directions.

[25] Our simulation study of λ_{eff} was motivated by its connection to strain hardening in a microscopic theory by K. Chen and K. S. Schweizer, private communication and unpublished.

[26] B.-Q. Luan and M. O. Robbins, unpublished.

[27] A similar collapse is not achieved for the total stress, which has smaller fluctuations.

[28] G. W. Adams and R. J. Ferris, J. Polym.. Sci. Part B - Polym. Phys. **26**, 433 (1988).

[29] O. B. Salamatina, G. W. H. Höhne, S. N. Rudnev, and E. F. Oleinik, Thermochimica Acta **247**, 1 (1994).

[30] E. F. Oleinik, S. N. Rudnev, O. B. Salamatina, S. V. Shenogin, M. I. Kotelyanskii, T. V. Paramzina, and S. I. Nazarenko, e-Polymers **029** (2006).